separations

MDPI

Article

Exploring Anti-Inflammatory Components in Dachengqi Tang Combining Bio-Affinity Ultrafiltration LC-MS with Cyclooxygenase-2

Ping Cai [1,†], Xiaowen Hua [2,3,†], Zhou Wu [1,†], Renai Fu [2,3,†], Meng Zhang [2,3], Junling Zhu [1], Ziqing Wu [2], Lutfun Nahar [4,*], Xiaoyu Dai [1,*], Mingquan Guo [2,3,*]

[1] Ningbo No.2 Hospital, Ningbo 315000, China; caipingxs@163.com (P.C.); nbeywz1889@126.com (Z.W.); zhujunling009@163.com (J.Z.)
[2] Laboratory of Advanced Theranostic Materials and Technology, Ningbo Institute of Materials Technology and Engineering, Chinese Academy of Sciences, Ningbo 315201, China; huaxiaowen@nimte.ac.cn (X.H.); furenai@nimte.ac.cn (R.F.); zhangmeng123@nimte.ac.cn (M.Z.); wuzq0907@163.com (Z.W.)
[3] Zhejiang International Scientific and Technological Cooperative Base of Biomedical Materials and Technology, Zhejiang Engineering Research Center for Biomedical Materials, Ningbo Cixi Institute of Biomedical Engineering, Cixi 315300, China
[4] Laboratory of Growth Regulators, Palacký University and Institute of Experimental Botany, The Czech Academy of Sciences, Šlechtitelů 27, 77200 Olomouc, Czech Republic
* Correspondence: profnahar@outlook.com (L.N.); daixiaoyu1968@163.com (X.D.); guomq@wbgcas.cn (M.G.)
† These authors contributed equally to this work.

Abstract

Postoperative ileus (POI) is a common gastrointestinal motility disorder involving intestinal inflammation and mucosal barrier dysfunction. Dachengqi Tang (DCQT), a traditional herbal formula, has demonstrated anti-inflammatory and intestinal protective effects, but its potentially active constituents and their relationships with POI-associated inflammatory proteins remain incompletely characterized. This study used bioaffinity ultrafiltration coupled with liquid chromatography–mass spectrometry (UF-LC-MS) to screen DCQT constituents retained in the presence of cyclooxygenase-2 (COX-2) and C-X-C motif chemokine ligand 1 (CXCL1). Selected candidates were further evaluated by molecular docking against COX-2 and by cell-based cytokine assays. LC-MS analysis indicated that the screened constituents mainly comprised flavonoids, anthraquinones, and related phytochemicals. Four candidates-hesperidin, naringin, rhein, and 6-methyl-aloe-emodin-were prioritized based on the ultrafiltration screening. Docking predicted favorable interactions of hesperidin and naringin with COX-2. In LPS-stimulated THP-1-derived macrophages, all four candidates reduced the measured levels of interleukin-6, interleukin-1β, and tumor necrosis factor-α. Overall, the findings prioritize candidate anti-inflammatory constituents of DCQT and provide preliminary evidence for further investigation of COX-2 docking predictions and CXCL1-associated ultrafiltration signals.

Keywords: bioaffinity ultrafiltration; Dachengqi Tang; anti-inflammatory activity; postoperative ileus

Academic Editors: Javier Saurina and Rosa María Alonso

Received: 14 September 2026
Revised: 28 October 2026
Accepted: 2 November 2026
Published: 4 November 2026

Copyright: © 2026 by the authors. Licensee MDPI, Basel, Switzerland. This article is an open access article distributed under the terms and conditions of the Creative Commons Attribution (CC BY) license.

1. Introduction

Postoperative ileus (POI) is a common complication after colorectal surgery, with an incidence of approximately 10-25% [1,2]. It can significantly delay patient recovery. The pathogenesis of POI is complex and involves multiple physiological processes, including impaired neural regulation of the gut and inflammatory responses. Studies have shown that POI has a two-phase pathological pattern. In the early stage, it is primarily characterized by neural dysfunction of intestinal smooth muscle, leading to reduced motility [3]. In the later stage, local and systemic inflammation become dominant, with cyclooxygenase-2 (COX-2) and the chemokine CXCL1 playing key roles in this process [1]. COX-2 is a critical enzyme for the production of prostaglandin E_2 (PGE_2). It converts arachidonic acid to prostaglandin G2 (PGG2) and then to prostaglandin H2 (PGH2). This process promotes the buildup of inflammatory cells and leads to tissue damage [4]. COX-2 expression is significantly increased in patients with postoperative intestinal obstruction. Elevated COX-2 expression is associated with abnormal intestinal blood flow, increased release of inflammatory mediators, and impaired intestinal motility. Inhibiting COX-2 activity can help reduce prostaglandin-driven inflammation and alleviate POI symptoms. CXCL1 primarily acts through CXCR2 and has been implicated in ileus-associated inflammation and impaired intestinal contractility [5]. We therefore selected CXCL1 as an exploratory screening bait to investigate whether DCQT constituents might interact with the chemokine itself. This disease-based rationale does not establish CXCL1 as a direct small-molecule target.

Medicinal plants are important sources of chemically diverse phytochemicals, including flavonoids, anthraquinones, phenolic compounds, terpenoids, alkaloids, and volatile constituents. Many of these compounds have been investigated for their potential to modulate inflammatory mediators, oxidative responses, and inflammation-related signaling processes [6–8]. Both nonvolatile phytochemicals and essential-oil constituents contribute to the broad biological activities reported for medicinal plants [7,8]. However, the chemical complexity of medicinal plant preparations makes it difficult to determine which constituents are associated with a particular biological activity, highlighting the need for analytical strategies that can characterize complex chemical profiles and prioritize potentially bioactive compounds.

Dachengqi Tang (DCQT, Major Purgative Decoction) is a classical traditional Chinese medicine (TCM) formula first documented by Zhang Zhongjing in the Shang Han Lun [9]. It has traditionally been used for Yangming-Fu excess syndrome, which is characterized by symptoms such as constipation, abdominal distension, abdominal pain, and a firm abdomen. Although some of these symptoms overlap with those observed in POI or intestinal obstruction, the traditional syndrome should not be regarded as equivalent to the modern clinical diagnosis of POI because their diagnostic frameworks and pathological definitions differ. Contemporary studies have investigated the effects of DCQT and its modified formulations on gastrointestinal motility, intestinal inflammation, and postoperative recovery [10,11]. DCQT consists of *Rheum palmatum L.* (rhubarb root), Magnolia officinalis Rehder & E.H. Wilson (magnolia bark), *Citrus aurantium L.* (immature bitter orange), and mirabilite (natural sodium sulfate). According to TCM theory, the formula promotes qi movement, relieves stagnation, and clears internal heat. Modern pharmacological studies suggest that DCQT may regulate gastrointestinal motility and inflammatory responses through multiple pathways [10,11]. In an LPS-induced acute lung injury model, DCQT reduced the levels of pro-inflammatory mediators, including IL-6, IL-8, and TNF-α, and altered the expression of aquaporins AQP-1 and AQP-5 [12]. Although this study provides evidence of the anti-inflammatory activity of DCQT, its findings were obtained in a non-intestinal preclinical model and therefore do not directly demonstrate ef-

ficacy in POI. Taken together, these studies provide a rationale for investigating the potential relevance of DCQT to inflammation and gastrointestinal dysfunction associated with POI. However, the available evidence does not establish that its traditional indications are equivalent to POI or that its effects are mediated through specific molecular targets. The principal anti-inflammatory constituents of DCQT and their contributions to its overall activity remain incompletely characterized. Because DCQT contains numerous constituents that may act through multiple pathways, identifying compounds associated with selected inflammation-related proteins remains challenging. In particular, whether individual DCQT constituents interact with COX-2 or CXCL1 and whether such interactions have functional consequences have not been fully determined. Therefore, the present study used protein affinity ultrafiltration coupled with LC-MS to prioritize candidate constituents associated with COX-2 and CXCL1 for further investigation.

Modern analytical techniques have facilitated the use of protein-based screening methods to investigate bioactive constituents in traditional Chinese medicine formulas. Protein affinity ultrafiltration coupled with liquid chromatography-mass spectrometry (UF-LC-MS) can enrich constituents retained in the presence of a selected protein and thereby prioritize candidate ligands from complex herbal extracts [13–15]. Molecular docking can provide computational predictions of possible binding poses, interaction sites, and relative docking scores, but these predictions require experimental confirmation [16]. The present study combines protein-affinity ultrafiltration using COX-2 and CXCL1, LC-MS analysis, molecular docking against COX-2, and cell-based assays to prioritize candidate anti-inflammatory constituents of DCQT. The aims were (1) to prioritize candidate anti-inflammatory constituents showing protein-associated retention in the COX-2 and CXCL1 ultrafiltration assays; (2) to examine predicted interaction patterns of selected compounds with COX-2 and generate hypotheses for further investigation; and (3) to provide preliminary evidence for further study of the anti-inflammatory activity of DCQT.

2. Materials and Methods

2.1. Extraction of Medicinal Materials and Sample Preparation

The traditional decoction was prepared according to the method described in Shang Han Lun, with minor modifications. The ingredients were Da Huang (lot 240801; Jiangxi Zhongkang Chinese Herbal Pieces Co., Ltd., Yichun, China), Hou Po (lot 250605571; Kangmei Pharmaceutical Co., Ltd., Puning, China), Zhi Shi (Kangmei Pharmaceutical Co., Ltd., Puning, China), and Mang Xiao (lot 240503081; Kangmei Pharmaceutical Co., Ltd., Puning, China). For DCQT, Zhi Shi (60 g), Hou Po (75 g), and Da Huang (60 g) were crushed and soaked in purified water (2000 mL) for 30 min. The mixture was then decocted twice, each time for 1.5 h. After the second decoction, Mang Xiao (40 g) was added and thoroughly stirred using residual heat. The solution was cooled, filtered, and concentrated under vacuum at 60 °C until the volume was reduced to approximately 200 mL. The concentrated product was frozen, freeze-dried for 48 h, and ground into a fine powder. The powder was passed through a 100-mesh sieve and stored in a desiccator until use.

2.2. Analysis and Putative Identification of DCQT Constituents

An accurately weighed portion of the freeze-dried DCQT extract (1.0 g) was dissolved in 15 mL of methanol, and the volume was adjusted to 25 mL with methanol. The solution was ultrasonicated for 30 min to obtain an extract concentration of 40 mg/mL and was stored at 4 °C until analysis. The sample was desalted using a C18 solid-phase extraction cartridge (Agilent Technologies, Beijing, China) to reduce interference from mirabilite

(Mang Xiao). The desalted extract was subsequently diluted to 4 mg/mL for LC-MS analysis.

Chromatographic separation was performed using an Agilent 1290 UPLC system coupled to an Agilent 6545 Q-TOF mass spectrometer (Agilent Technologies, Santa Clara, CA, USA). Separation was carried out on an EC-C18 column (3.0 × 150 mm, 2.7 μm) maintained at 25 °C. The mobile phases consisted of 0.1% formic acid in water (A) and 0.1% formic acid in acetonitrile (B). The flow rate was 0.3 mL/min, and the injection volume was 5 μL.

The same gradient program was used in positive- and negative-ion modes. The proportion of mobile phase B increased linearly from 5% to 50% during 0-12 min and then increased to 90% at 15 min. It was maintained at 90% from 15 to 35 min, changed to 95% at 35 min, and was maintained at 95% until 45 min. The proportion of B was returned to 5% at 45 min and maintained at 5% from 45 to 50 min for column re-equilibration.

The mass spectrometer was operated in positive- and negative-ion electrospray ionization modes. The ion-source parameters were as follows: capillary voltage, 3500 V; drying gas temperature, 350 °C; drying gas flow rate, 8 L/min; nebulizer pressure, 35 psi; and fragmentor voltage, 175 V. Data were acquired in Auto MS/MS mode at 3 spectra/s over an *m*/*z* range of 50-1100. Collision energies of 10, 20, and 40 V were used for MS/MS acquisition. Real-time reference-mass correction was performed using the Agilent Tune Mix/Reference Ion solution. The reference ions were *m*/*z* 121.0508 and 922.0098 in positive-ion mode and *m*/*z* 112.9855 and 1033.9881 in negative-ion mode.

The detected constituents were putatively annotated by comparing accurate precursor masses, molecular formulas, isotope patterns, and characteristic MS/MS fragments with the Agilent PCDL libraries, including the ForensicsTox AM PCDL and LC/Q-TOF Applied Markets PCDL, the Human Metabolome Database, and previously published literature. A precursor-mass error of less than 10 ppm was used as the acceptance criterion for molecular-formula assignment. Because authentic reference standards were not used, the reported compound names represent putative annotations rather than confirmed structural identifications. Features satisfying the accurate-mass and MS/MS criteria were assigned as putative Level 2 annotations, whereas entries that did not meet the predefined mass-error criterion were retained as unresolved features pending re-examination of the raw data.

2.3. Protein Affinity Ultrafiltration Screening with COX-2 and CXCL1

Protein affinity ultrafiltration was used to enrich DCQT constituents retained in the presence of COX-2 or CXCL1 and thereby prioritize candidate protein-associated ligands. The procedure comprised protein-extract incubation, ultrafiltration and elution, followed by UPLC-Q-TOF-MS/MS analysis. The procedure was adapted from previously reported methods [17,18]. The COX-2 and CXCL1 experiments were conducted separately.

DCQT extract was prepared in PBS (pH 7.4) at a concentration of 4 mg/mL, as described in Section 2.2. COX-2 and CXCL1 were separately prepared in buffer containing 0.01% BSA. For each incubation, 150 μL of DCQT extract was mixed with 20 μL of the COX-2 solution containing 5 μg of protein or 20 μL of the CXCL1 solution containing 10 μg of protein. PBS (100 μL, pH 7.4) was then added to each mixture, followed by incubation at 37 °C for 40 min.

For the control preparations, COX-2 and CXCL1 were separately heat-treated by boiling for 15 min. Following incubation, the native-protein and heat-treated-protein mixtures were transferred to separate Amicon Ultra centrifugal ultrafiltration devices (Sigma-Aldrich, St. Louis, MO, USA) containing regenerated-cellulose membranes. A 30 kDa molecular-weight-cutoff device (Cat. No. UFC5030, Merck Millipore, Billerica, MA, USA) was

used for the COX-2 mixtures, whereas a 3 kDa molecular-weight-cutoff device (Cat. No. UFC5003, Merck Millipore, Billerica, MA, USA) was used for the CXCL1 mixtures.

Centrifugation was performed using a TGL-18M refrigerated centrifuge (BIO-RIDGE/Lu Xiang Yi, Shanghai, China) equipped with a No. 2 rotor that accommodates 24 tubes of 1.5/2.2 mL. The rotor has a maximum speed of 16,000 rpm and a maximum relative centrifugal force of 23,755× *g*. Following protein - extract incubation, the samples were centrifuged at 11,000× *g* and 4 °C for 10 min. The retained fractions were washed three times with 200 μL of PBS (pH 6.8), with centrifugation at 11,000× *g* and 4 °C for 10 min after each wash.

The protein-associated constituents retained by the ultrafiltration membrane were eluted by adding 200 μL of 90% aqueous methanol. After standing for 10 min, the devices were centrifuged at 11,000× *g* and 4 °C for 10 min. The elution procedure was performed twice, and the resulting filtrates were pooled. The pooled eluates were dried under nitrogen and reconstituted in 100 μL of methanol for subsequent UPLC-Q-TOF-MS/MS analysis.

The binding degree (BD) was calculated as a descriptive measure of the difference in LC-MS peak recovery between the native-protein and heat-treated-protein preparations:

$$\text{Binding Degree (\%)} = (S_1 - S_2)/S_1 \times 100$$

S_1 is the LC-MS peak area of a constituent recovered after incubation with the native protein, and S_2 is the corresponding peak area after incubation with the heat-treated protein. Native- and heat-treated-protein preparations were processed identically, and retained fractions were washed three times with PBS to reduce background retention. BD reflects relative protein-associated retention under the ultrafiltration conditions.

Each COX-2 and CXCL1 affinity ultrafiltration experiment was conducted independently once. Therefore, the BD values were used for descriptive candidate prioritization and were not subjected to inferential statistical analysis. Because heat treatment may alter protein conformation and nonspecific ligand retention, the native-versus-heat-treated comparison cannot completely exclude nonspecific adsorption to the protein, membrane, or device surfaces.

2.4. UPLC-Q-TOF-MS/MS Analysis

The eluates obtained from the affinity ultrafiltration experiments were analyzed by UPLC-Q-TOF-MS/MS using the instrument settings described in Section 2.2.

2.5. Molecular Docking Simulation

Molecular docking against COX-2 was performed using AutoDock Vina 1.2.0. The three-dimensional structure of COX-2 (PDB ID: 3LN1) was retrieved from the RCSB Protein Data Bank (www.rcsb.org), and celecoxib was used as a computational reference. The 3D structures of the ligands were generated using ChemBio3D Ultra 12.0, and the lowest-energy conformations were selected for docking [19,20]. The protein and ligands were prepared using AutoDockTools 1.5.7 (Scripps Research Institute, San Diego, CA, USA), including removal of water molecules and the original ligand, addition of hydrogen atoms, and energy minimization. A semiflexible docking protocol was applied, with the protein held rigid and the ligand flexible. The grid box was centered at x = 22.5, y = 18.7, and z = 15.2, with dimensions of 30 Å × 30 Å × 30 Å, covering the ligand-binding pocket of the selected COX-2 structure. The exhaustiveness parameter was set to 16. The best-scoring pose, determined by the lowest predicted binding energy, was retained for analysis. The docking protocol was validated by redocking the co-crystallized ligand, which yielded an RMSD of 0.85 Å.

2.6. Cell Culture and Treatment

THP-1 cells were seeded in 6-well plates at a density of 2.5×10^5 cells/mL and cultured in RPMI 1640 medium. The THP-1 cell line was purchased from BDBIO (Shanghai, China; Cat. No. C5157). The cells were then treated with 100 ng/mL phorbol 12-myristate 13-acetate (PMA) for 48 h to induce differentiation into macrophages. Subsequently, the cells were treated for 24 h with various concentrations of the test compounds: 6-methyl-aloe-emodin (5, 10, 20 μM), rhein (10, 20, 40 μM), naringin (12.5, 25, 50 μM), and hesperidin (12.5, 25, 50 μM). Aspirin at 100 μM was used as a control. The cells were then stimulated with 100 ng/mL lipopolysaccharide (LPS) for 6 h to induce an inflammatory response. The cell culture supernatant was collected, and the levels of inflammatory cytokines IL-6, IL-1β, and TNF-α were measured using ELISA kits.

2.7. Statistical Analysis

The cell-based experiments were performed in triplicate (three biological replicates, each with two technical replicates). Data are expressed as mean ± standard deviation (SD). Normality was assessed using the Shapiro–Wilk test, with $p > 0.05$ considered as indicating a normal distribution. For multiple-group comparisons, one-way analysis of variance (ANOVA) followed by Tukey's honest significant difference (HSD) post hoc test was used. A p value < 0.05 was considered statistically significant. All statistical analyses were conducted using SPSS 17.0.

3. Results

3.1. Putative Identification of Chemical Constituents in Dachengqi Tang

Compounds were putatively annotated by matching the MS and MS/MS fragment data with reference information from previous studies and publicly available databases, including PubChem and MassBank. LC-MS analysis yielded 21 putative annotations in negative-ion mode and 18 in positive-ion mode. The chromatograms are shown in Figures 1 and 2. To characterize the DCQT extract, high-resolution mass spectrometry (HRMS) and MS/MS fragment interpretation were used. The putatively annotated compounds belonged to various classes, including flavonoids, phenylpropanoid glycosides, anthraquinones, lignans, and alkaloids. To broaden detection, both positive-ion mode (ESI^+) and negative-ion mode (ESI^-) were employed. The detailed chemical information for each compound is provided in Tables 1 and 2.

Table 1. Qualitative analysis of compounds in Dachengqi Tang extract under negative ion mode.

Peak	RT (min)	Measured *m*/*z*	Theoretical *m*/*z*	Identification	Molecular Formula	MS/MS (*m*/*z*)	Error (ppm)	Source/Reference
1	2.545	341.1088	341.1089	Sucrose	$C_{12}H_{22}O_{11}$	89.0238, 71.0135, 101.0240, 150.0421, 113.0241, 179.0546, 133.0161	−0.40	HMDB0000258 (https://hmdb.ca/metabolites/HMDB0000258, accessed on 21 October 2026)
2	17.111	357.0591	357.0616	Succinyldisalicylic acid	$C_{18}H_{14}O_8$	289.0711, 245.0812, 311.0531, 137.0240, 125.0243, 179.0349, 203.0713, 109.0292, 123.0451, 137.0241, 151.0396	−7.00	HMDB0251143 (https://hmdb.ca/metabolites/HMDB0251143, accessed

							on 21 October 2026)
3	17.661	289.0719	289.0718	(-)-Epicatechin	$C_{15}H_{14}O_6$	245.0817, 205.0503, 179.0346, 125.0245, 109.0291, 109.0294, 151.0395, 203.0716, 245.0816, 137.0244, 179.0345, 221.0816	0.48	[21], HMDB0001871 (https://hmdb.ca/metabolites/HMDB0001871, accessed on 21 October 2026)
4	21.566	371.1354	371.1348	Perilloside E	$C_{17}H_{22}O_9$	163.0759, 174.9563, 57.0348, 101.0245, 113.0239, 57.0346, 130.9657	1.62	HMDB0041115 (https://hmdb.ca/metabolites/HMDB0041115, accessed on 21 October 2026)
5	22.123	445.0783	445.0776	Rhein-8-O-β-D-glucopyranoside	$C_{21}H_{18}O_{11}$	165.0406, 211.0400, 239.0356, 283.0255, 307.0249	1.49	[22]
6	26.686	593.1511	593.1512	Vicenin-2	$C_{27}H_{30}O_{15}$	353.0667, 33.0772, 473.1088, 325.0715, 503.1202,297.0765	−0.16	[23]
7	27.041	623.1987	623.1981	Forsythoside I	$C_{29}H_{36}O_{15}$	161.0242, 135.0446, 315.1084, 461.1677	0.89	[24], HMDB0252460
8	28.312	477.1411	477.1402	Calceolarioside B	$C_{23}H_{26}O_{11}$	313.0563, 169.0139, 151.0034, 125.0242, 169.0140, 125.0242, 151.0034	1.60	PubChem CID 5273567 (https://pubchem.ncbi.nlm.nih.gov/compound/5273567, accessed on 21 October 2026)
9	28.994	579.1724	579.1919	Naringin	$C_{27}H_{32}O_{14}$	292.0609, 313.0712, 151.0036, 271.0613, 119.0502, 193.0137, 295.0610	0.81	[25]
10	29.555	609.1834	609.1825	Hesperidin	$C_{28}H_{34}O_{15}$	301.0718, 325.0717, 125.0243, 151.0031, 164.0111, 199.0398, 242.0583, 257.0816, 286.0480	1.49	[25]
11	30.592	193.0509	193.0506	cis-Ferulic acid	$C_{10}H_{10}O_4$	134.0369, 161.0241, 178.0267, 106.0423, 77.0390, 133.0293, 104.0260, 77.0395	1.39	HMDB0240705 (https://hmdb.ca/metabolites/HMDB0240705, accessed on 21 October 2026)
12	31.657	471.1659	-	-	-	145.0292, 307.0820, 163.0396, 119.0498,		

						187.0397, 205.0505, 247.0605,117.0340		
13	32.19	407.1350	407.1348	Torachrysone-8-O-β-D-glucopyranoside	$C_{20}H_{24}O_9$	245.0819, 278.9166, 230.0593, 193.7536, 255.3688, 230.0581, 215.0351, 282.7142	0.60	[22]
14	32.545	431.0983	431.0984	Sophoricoside	$C_{21}H_{20}O_{10}$	269.0456, 293.0457, 311.0560,225.0554, 2	−0.16	[26]
15	37.395	283.026	283.0612	Rhein	C15H8O6	139.0557, 183.0455, 211.0402, 239.0350	2.79	[27]
16	38.58	283.0611	283.0612	Genkwanin	$C_{16}H_{12}O_5$	190.9445, 240.0422, 148.9565, 268.0373, 254.0571, 104.9673, 212.0477, 184.0528, 254.7846	−0.34	HMDB0252684 (https://hmdb.ca/metabolites/HMDB0252684, accessed on 21 October 2026)
17	39.6	253.0873	253.0870	Magnolaldehyde D	$C_{16}H_{14}O_3$	207.0796, 235.0766, 253.0765, 207.0811, 194.0348, 243.3266, 208.0544, 233.0625, 180.0587,219.4296	1.11	[28]
18	40.178	311.1683	311.1653	Triptophenolide	$C_{20}H_{24}O_3$	119.0508, 183.0128, 225.0600	9.74	PubChem CID 173273 (https://pubchem.ncbi.nlm.nih.gov/compound/173273, accessed on 21 October 2026)
19	40.888	194.0825		-	-	149.0607, 164.0842, 179.0585, 108.0213, 148.0530, 178.0504, 121.0654,134.0372		
20	41.421	269.0458	269.0455	Aloe emodin	$C_{15}H_{10}O_5$	225.0553, 241.0497, 182.0371, 197.0600, 210.0318,105.0335	0.94	[22]
21	41.626	265.1235	265.1234	Honokiol	$C_{18}H_{18}O_2$	247.1127, 245.0969, 223.0763, 204.0582, 119.0500,91.0548	0.36	[28], HMDB0253212 (https://hmdb.ca/metabolites/HMDB0253212, accessed on 21 October 2026)

Table note. HMDB, Human Metabolome Database; CID, PubChem Compound Identifier; PCDL, Personal Compound Database and Library. "-" indicates that no verified database accession number is provided for the proposed compound.

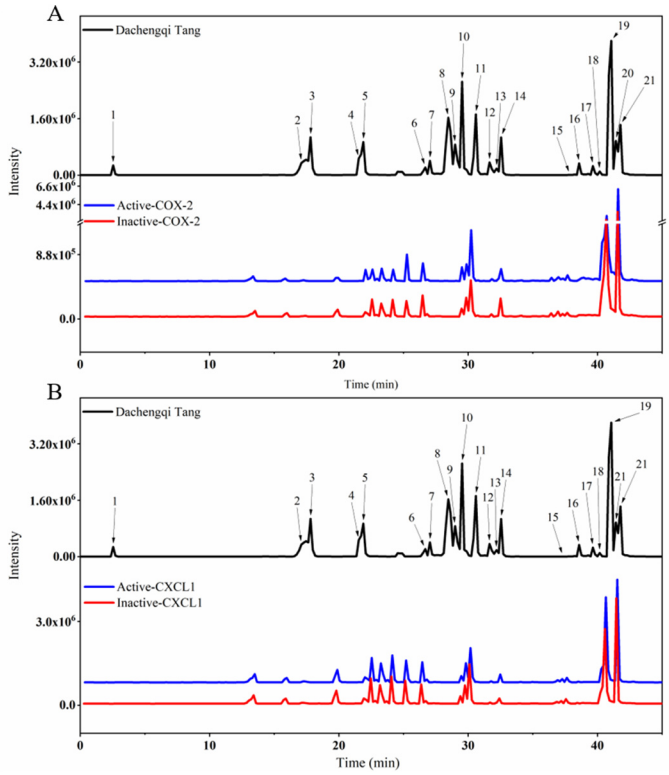


Figure 1. Extracted-ion chromatogram (EIC) of Dachengqi Tang extract in negative-ion mode. The black line represents the chromatogram of the compound extract before ultrafiltration, while the red and blue lines represent the chromatograms of the compound extract after ultrafiltration with (**A**) COX-2 and (**B**) CXCL1.

DCQT contains a diverse range of flavonoids, mainly originating from Aurantii Fructus Immaturus (Zhi Shi) and other herbal components. The putatively annotated flavonoids include sophoricoside, vicenin-2, hesperidin, naringin, (-)-Epicatechin, isosinensetin, 3,3′,4′,5,7,8-hexamethoxyflavone, hesperetin, and genkwanin, with naringin and hesperidin being the predominant flavonoid glycosides.

Table 2. Qualitative analysis of compounds in Dachengqi Tang extract in positive-ion mode.

Peak	RT (min)	Measured *m*/*z*	Theoretical *m*/*z*	Identification	Molecular Formula	MS/MS (*m*/*z*)	Error (ppm)	Source/Reference
1	2.546	143.0946	143.0946	proline betaine	$C_7H_{13}NO_2$	58.0661, 84.0827, 144.1062, 57.0567, 91.0434, 135.0712, 107.0514, 121.0672	0.00	HMDB0004827 (https://hmdb.ca/metabolites/HMDB0004827, accessed on 21 October 2026)
2	3.256	168.1019	168.1019	p-Synephrine	$C_9H_{13}NO_2$	91.0573, 119.0528, 135.0722, 135.0723, 107.0512, 51.0244, 65.0407, 120.0473	0.00	HMDB0004826 (https://hmdb.ca/m

								etabo-lites/HMDB0004826, accessed on 21 October 2026)
3	5.031	364.1351	364.1351	N-Biotinyl-4-amino-benzoic acid	$C_{17}H_{21}N_3O_4S$	149.0641, 167.0758, 123.0352, 85.0310, 263.1028, 180.0899, 263.1028	6.87	HMDB0248835 (https://hmdb.ca/metabolites/HMDB0248835, accessed on 21 October 2026)
4	9.647	344.1827	344.1856	-	$C_{20}H_{25}NO_4$	107.0541, 165.0986, 180.0951, 85.0327, 145.0562, 127.0446, 69.0375	−8.43	Agilent PCDL
5	10	291.0863	291.0863	(-)-Epicatechin	$C_{15}H_{14}O_6$	103.0438, 225.0036, 123.0501, 139.0460, 109.0669, 127.0927, 81.0471	0.00	HMDB0001871 (https://hmdb.ca/metabolites/HMDB0001871, accessed on 21 October 2026)
6	12.84	285.0504	285.0504	6-Methyl-aloe-emodin	$C_{16}H_{12}O_5$	101.0987, 241.0590, 267.0163, 72.0734, 146.0669, 188.0786, 183.0519, 155.0560, 121.0192, 139.0443, 167.0553, 211.0271	0.00	[27]
7	14.29	581.1888	581.1865	Naringin	$C_{27}H_{32}O_{14}$	273.0860, 419.1454, 435.1392, 401.1346, 315.0978, 129.0604, 195.0369, 345.1079, 413.1343, 303.0971, 177.0621, 195.0371	3.96	[29], HMDB0002927 (https://hmdb.ca/metabolites/HMDB0002927, accessed on 21 October 2026)
8	15.33	611.1913	611.1970	Hesperidin	$C_{28}H_{34}O_{15}$	303.0967, 449.1559, 465.1514, 345.1073, 431.1450, 465.1514, 129.0602, 195.0369, 303.0971, 71.0527	−9.33	[25], HMDB0002927 (https://hmdb.ca/me-

								tabolites/HMDB0002927, accessed on 21 October 2026)
9	20.12	247.1071	247.1077	N-Acetyltryptophan	$C_{13}H_{14}N_2O_3$	229.0952, 205.0950, 201.0994, 214.0714, 158.0797, 115.0594, 171.0522, 186.0760, 130.0836	−2.43	HMDB0013713 (https://hmdb.ca/metabolites/HMDB0013713, accessed on 21 October 2026)
10	23.32	285.0872	285.0870	Phenytoin catechol	$C_{15}H_{12}N_2O_4$	211.0848, 242.0676, 267.0758, 168.0651, 196.0604, 140.0680, 77.0428, 224.0520	0.70	HMDB0060865 (https://hmdb.ca/metabolites/HMDB0060865, accessed on 21 October 2026)
11	23.85	513.1648	513.1603	3-(4-Hydroxy-3-methoxyphenyl)-1,2-propanediol 2-O-(galloyl-glucoside)	$C_{23}H_{28}O_{13}$	103.0436, 233.0053, 331.0760, 349.0872, 393.0771, 167.1253, 149.1138, 185.1366, 349.0870	8.77	HMDB0036376 (https://hmdb.ca/metabolites/HMDB0036376, accessed on 21 October 2026)
12	24.23	226.1931	226.1914	-	$C_{12}H_{23}N_3O$	208.1721, 180.1767, 163.1494, 198.1884, 55.0527, 83.0846, 69.0690	7.52	Agilent PCDL
13	27.76	373.1271	373.1282	Isosinensetin	$C_{20}H_{20}O_7$	312.0855, 329.1137, 343.0930, 358.1155, 343.0929, 315.0972, 357.1004, 153.0246, 181.0209	−2.95	[29]
14	29.22	274.2016	274.2013	Heptanoyl-L-carnitine	$C_{14}H_{27}NO_4$	57.0623, 70.0684, 88.0673, 106.0907, 230.2568, 256.2740, 116.0771, 79.0579, 131, 0609, 149.0673	1.09	Agilent PCDL
15	29.71	290.1961	290.1962	3-Hydroxyheptanoylcarnitine	$C_{14}H_{27}NO_5$	74.0638, 88.0797, 122.0866, 242.2574, 242.2580, 122.0866,	−0.34	Agilent PCDL

						56.0524, 228.2410, 272.2685		
16	30.48	403.1352	403.1387	5,6,7,8,3,4-Hexamethoxyflavone	$C_{21}H_{22}O_8$	373.1032, 388.1280, 327.0965, 342.1221, 355.0931, 373.1035, 211.0329, 183.0362, 330.0857, 358.0550	−8.68	[29]
17	33.62	302.079	302.0788	Hesperetin	$C_{16}H_{14}O_6$	57.0732, 70.0691, 88.0802, 106.0910, 284.2832, 149.9897	0.66	[29]
18	37.02	365.1482	-	-	-	243.1081, 105.0237112.0915, 136.0656, 177.1006, 228.0741, 349.7267	-	-

Table note. HMDB, Human Metabolome Database; CID, PubChem Compound Identifier; PCDL, Personal Compound Database and Library. "-" indicates that no verified database accession number is provided for the proposed compound.

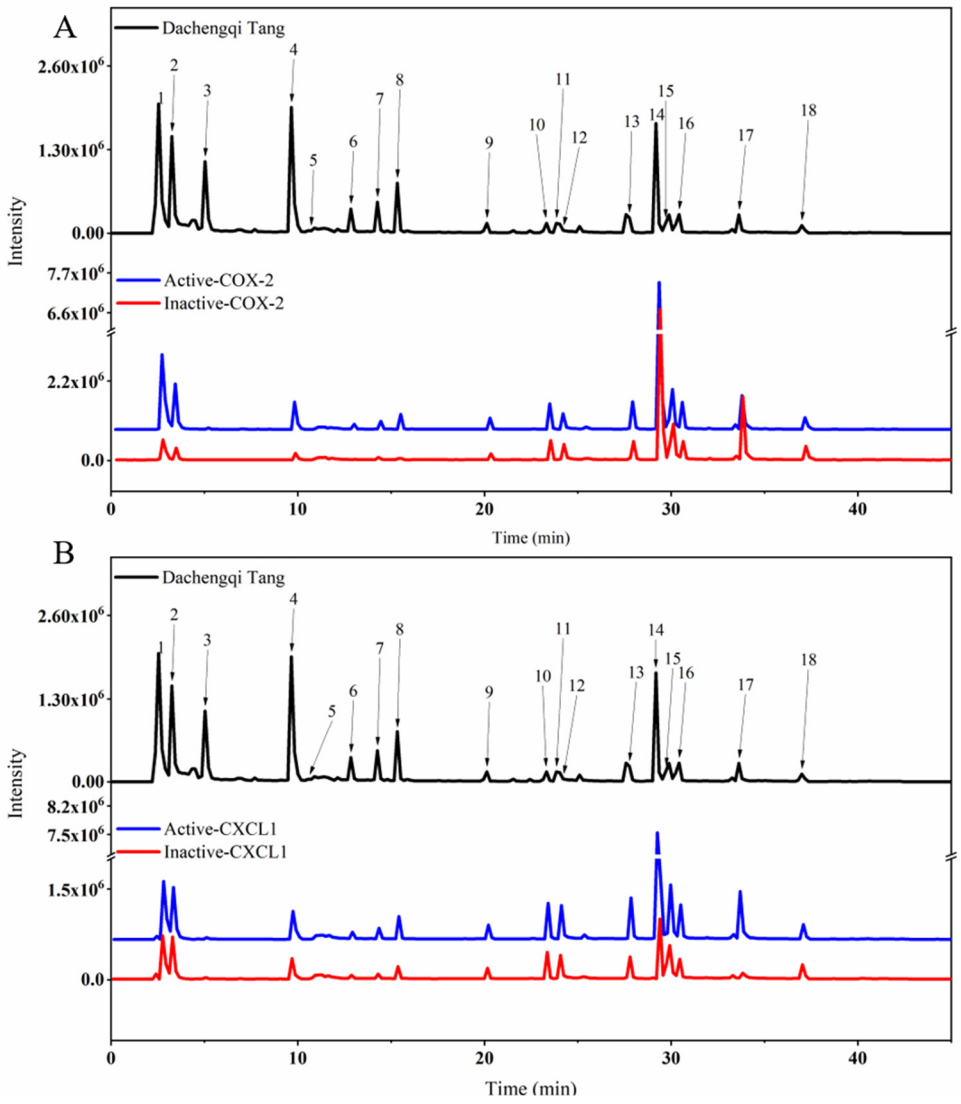


Figure 2. Extracted-ion chromatogram (EIC) of Dachengqi Tang extract in positive-ion mode. The black line represents the chromatogram of the compound extract before ultrafiltration, while the red

and blue lines represent the chromatograms of the compound extract after ultrafiltration with (**A**) COX-2 and (**B**) CXCL1.

In positive-ion mode, naringin ($C_{27}H_{32}O_{14}$) produced a $[M+H]^+$ ion at *m*/*z* 581.1888, and its main MS/MS fragment at *m*/*z* 273.0860 corresponded to the aglycone naringenin formed by the loss of a rhamnose-glucose disaccharide (308 Da). Similarly, hesperidin ($C_{28}H_{34}O_{15}$) generated a $[M+H]^+$ ion at *m*/*z* 611.1913 and a characteristic aglycone fragment at *m*/*z* 303.0967 (hesperetin). Both glycosides exhibited typical O-diglycoside fragmentation, including sequential sugar loss and aromatic ring cleavage producing diagnostic ions such as *m*/*z* 153. Several aglycone flavonoids were also detected, covering flavan-3-ols, polymethoxy flavones, and simple flavones. (-)-Epicatechin ($C_{15}H_{14}O_6$) appeared in both ionization modes. Polymethoxyflavones, such as isosinensetin ($C_{20}H_{20}O_7$) and 3,3′,4′,5,7,8-hexamethoxyflavone ($C_{21}H_{22}O_8$), showed strong hydrophobicity and distinctive MS fragmentation. Hesperetin ($C_{16}H_{14}O_6$) and genkwanin ($C_{16}H_{12}O_5$), two nonglycosylated flavonoids, further expanded the structural diversity of the flavonoid profile in DCQT.

One of the principal herbs in the DCQT formula, Radix et Rhizoma Rhei (Da Huang, rhubarb), provides the major anthraquinone constituents. Mass spectrometric analysis of the extract suggested multiple anthraquinone derivatives, including 6-methyl-aloe-emodin, physcion, rhein, rhein-8-O-β-D-glucopyranoside, torachrysone-8-O-β-D-glucopyranoside, and aloe-emodin, among others. These putative annotations illustrate the structural diversity of anthraquinone components in the extract. In positive-ion mode, peak 6 was provisionally annotated as 6-methyl-aloe-emodin ($C_{16}H_{12}O_5$) with $[M+H]^+$ at *m*/*z* 285.0504. Its MS/MS fragment ions at *m*/*z* 267.0390 and 241.0590 correspond to sequential losses of H_2O (18 Da) and CO (28 Da) from the parent ion, consistent with the anthraquinone scaffold's propensity to eliminate small neutral molecules. Similarly, peak 10 (Phenytoin catechol, $C_{15}H_{12}N_2O_4$, $[M+H]^+$ *m*/*z* ≈285.09) exhibited a comparable fragmentation pattern, with a fragment ion at *m*/*z* 267.0758, which indicates the presence of similarly labile substituents in its structure. In negative-ion mode, peak 20 was provisionally annotated as aloe-emodin ($C_{15}H_{10}O_5$) with an [M-H]- ion at *m*/*z* 269.0458. Its MS/MS fragment ions at *m*/*z* 241.0503 and 225.0553 reflect the typical fragmentation pattern of an anthraquinone core, characterized by sequential losses of CO and CO_2. Additionally, rhein ($C_{15}H_8O_6$) and its glycosides were also detected, further broadening the structural diversity of the anthraquinone compounds present.

Alkaloid features were also examined in DCQT; several of the proposed constituents may originate from Zhi Shi (immature bitter orange fruit). Chemical analysis suggested the presence of several representative alkaloids, including proline betaine, p-Synephrine, and magnoflorine. In positive-ion mode, p-Synephrine exhibited an $[M+H]^+$ ion at *m*/*z* 168.1019, corresponding to the molecular formula $C_9H_{13}NO_2$. Its MS/MS fragmentation yielded major fragment ions at *m*/*z* 135.0722, 119.0528, and 107.0523, which can be attributed to the cleavage of the catecholamine side chain and the formation of stable benzyl cation fragments on the aromatic ring. These features are consistent with the expected fragmentation behavior of synephrine's p-hydroxyphenethylamine backbone. proline betaine ($C_7H_{13}NO_2$) produced an $[M+H]^+$ ion at *m*/*z* 143.0946. The observed fragment ions at *m*/*z* 84.0827 and 58.0661 are tentatively assigned to a pyrrolidinium ring and a trimethylamine moiety, respectively, reflecting the structural characteristics of stachydrine as a proline betaine-type compound.

In addition to the primary classes of compounds described above, several other constituents were detected in the DCQT extract, underscoring the diversity of the formula's chemical composition. Honokiol (peak 21, $C_{18}H_{18}O_2$) was provisionally annotated as a representative Magnoliaceae biphenolic (lignan) derived from Magnolia officinalis bark (Hou

Po). In negative-ion mode, honokiol showed an $[M-H]^-$ ion at *m*/*z* 265.1235, and its fragmentation pattern suggested cleavage of the biphenylpropanoid structure (for example, loss of a propyl side chain yielding an *m*/*z* 247 fragment). In addition, a number of phenolic acids and glycosides were detected, such as methyl caffeate, forsythoside I, and calceolarioside B, whose origins require further confirmation.

In summary, the DCQT extract contains features provisionally assigned to flavonoids, anthraquinones, alkaloids, lignans, and triterpenoids. Honokiol was a representative putative lignan in the extract. In the LC-MS analysis, honokiol showed a strong signal in the ESI^+ mode. Its parent ion peak ($[M+H]^+$) appeared at *m*/*z* 265.124, and the fragment ions at *m*/*z* 119.050 and 223.076 matched the typical fragmentation pattern of lignans. Because of its hydrophobicity, honokiol showed a later retention time under reversed-phase chromatography conditions. The putative chemical profile is consistent with the diverse classes of constituents reported for DCQT. The biological contributions of individual features and possible interactions among them require further study.

3.2. Protein-Affinity Ultrafiltration Screening of DCQT Constituents

Using separate COX-2 and CXCL1 protein affinity ultrafiltration coupled with LC-MS assays, several provisionally annotated constituents of DCQT showed differences in recovered peak areas between the native-protein and heat-treated-protein preparations. The binding degree (BD) was calculated as a descriptive measure of relative protein-associated retention under the ultrafiltration conditions. Tables 3 and 4 present the BD values obtained for the COX-2 and CXCL1 preparations in positive- and negative-ion modes. These values were used to prioritize candidate constituents and should not be interpreted as quantitative binding affinities, evidence of specific binding, or functional inhibition of either protein.

Table 3. Binding-degree values of negative-ion features after COX-2 or CXCL1 protein affinity ultrafiltration.

Peak	Identification	BD (%)	
		Cox-2	CXCL1
1	Sucrose	7.45	16.55
3	(-)-Epicatechin	1.51	2.35
6	Vicenin-2	-	10.00
7	Forsythoside I	-	2.07
8	Calceolarioside B	-	0.54
9	Naringin	-	1.81
10	Hesperidin	48.29	-
11	cis-Ferulic acid	-	14.35
12	Limonin	31.48	7.24
13	Torachrysone-8-O-β-D-glucopyranoside	-	5.97
14	Sophoricoside	21.74	2.66
15	Rhein	32.77	-
16	Genkwanin	-	25.46
17	Magnolaldehyde D	20.12	9.77
18	Triptophenolide	51.35	64.34
20	Aloe emodin	4.71	8.00
21	Honokiol	38.80	0.52

The affinity ultrafiltration results showed differences in BD values among the provisionally annotated DCQT features recovered after incubation with COX-2 or CXCL1. For COX-2, several compounds showed high BD values, with 6-methyl-aloe-emodin (95.08%),

hesperidin (84.78%), naringin (67.77%), and N-biotinyl-4-aminobenzoic acid (83.96%) showing prominent native-versus-control differences. Compounds such as triptophenolide (51.35%), honokiol (38.80%), and limonin (31.48%) showed intermediate BD values, whereas a number of other constituents had low BD values (<10%). In contrast, the CXCL1 binding profile showed a different retention pattern, with hesperetin (83.42%), triptophenolide (64.34%), naringin (55.82%), 6-methyl-aloe-emodin (54.07%), and isosinensetin (45.44%) showing the highest BD values in the CXCL1 assay. The difference in hesperidin BD values between negative (48.29%) and positive (84.78%) ion modes in Tables 3 and 4 may reflect differences in ionization and peak integration between modes; the cause was not experimentally established. Mode-specific BD values are reported separately because they are not directly interchangeable. These features were prioritized for further investigation. Features with intermediate BD values such as hesperidin and genkwanin were also observed; low BD values do not establish a lack of biological activity. When comparing the two targets, several constituents, including 6-methyl-aloe-emodin, naringin, triptophenolide, and hesperidin, had elevated BD values in both assays, making them candidates for subsequent validation. The symbol "-" indicates that a BD value was not reported; it should not be interpreted as evidence of absent binding. The differing BD patterns may reflect assay-dependent retention and require confirmation by orthogonal methods. Overall, the BD data provide a preliminary ranking of protein-associated features and do not establish target selectivity or a cellular mechanism.

Table 4. Binding-degree values of positive-ion features after COX-2 or CXCL1 protein affinity ultrafiltration.

Peak	Identification	BD (%)	
		Cox-2	CXCL1
1	proline betaine	69.60	30.08
2	Synephrine	84.45	17.86
3	N-Biotinyl-4-aminobenzoic acid	83.96	56.75
5	(-)-Epicatechin	0.39	8.71
6	6-Methyl-aloe-emodin	95.08	54.07
7	Naringin	67.77	55.82
8	Hesperidin	84.78	45.71
9	N-Acetyltryptophan	47.97	29.42
10	Phenytoin catechol	25.63	26.75
11	3-(4-Hydroxy-3-methoxyphenyl)-1,2-propanediol 2-O-(galloyl-glucoside)	6.00	17.92
13	Isosinensetin	32.55	45.44
14	Heptanoylcarnitine	-	87.05
15	3-Hydroxyheptanoylcarnitine	1.42	19.82
16	3,3′,4′,5,7,8-Hexamethoxyflavone	31.55	44.66
17	Hesperetin	-	83.42

"-" indicates that the compound has no binding affinity.

3.3. COX-2 Molecular Docking Analysis

To characterize the predicted interactions of selected compounds with COX-2, representative candidates were selected for molecular docking based on their putative LC-MS annotations, peak areas, and binding-degree (BD) values in the positive- and negative-ion modes (Table 5). The docking analysis generated possible binding poses and interaction patterns with COX-2, as shown in Figure 3. The Ki values in Table 5 are docking-derived computational estimates intended only for relative, semiquantitative comparison under the same docking protocol. They should not be interpreted as experimentally measured

binding affinities or inhibitory constants and do not establish functional target inhibition. The docking results are hypothesis-generating and require direct experimental validation.

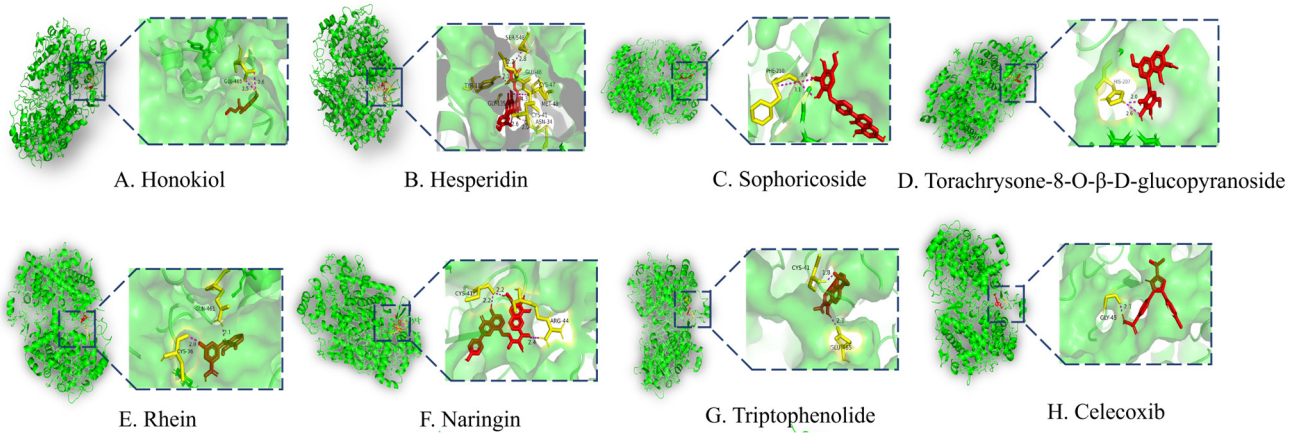


Figure 3. Predicted docking poses of selected Dachengqi Tang constituents with COX-2. Panels (**A**–**H**) show poses with COX-2, with celecoxib as a computational reference.

Table 5. Predicted docking interactions of selected ligands with COX-2.

Peaks	Enzymes	BE (kcal/mol)	Docking-Derived Ki Estimate	Hydrogen Bonds
Honokiol	COX-2	−5.97	41.88 μM	GLU465
Hesperidin	COX-2	−11.76	2.40 nM	TYR130, GLY135, GLU46, CYS47, CYS41, SER548, MET48, ASN34
Sophoricoside	COX-2	−10.43	22.47 nM	PHE210, GLN289
Torachrysone-8-*O*-*β*-D-glucopyranoside	COX-2	−8.96	271.64 nM	HIS207
Rhein	COX-2	−5.71	64.93 μM	CYS36, GLN461
Triptophenolide	COX-2	−8.40	691.55 nM	GLU465, CYS41
Naringin	COX-2	−11.26	5.59 nM	ARG44, CYS41
Positive control Celecoxib	COX-2	−7.58	2.78 μM	GLY45

The reported Ki values were estimated computationally from the docking scores and do not represent experimentally measured binding affinities or inhibitory constants.

Among the compounds evaluated, hesperidin and naringin showed the most favorable docking scores for COX-2. Hesperidin had a predicted binding energy of −11.76 kcal/mol and a docking-derived Ki estimate of 2.40 nM. Its predicted pose included multiple hydrogen-bonding interactions with Tyr130, Gly135, Glu46, Cys47, Cys41, Ser548, Met48, and Asn34. Naringin had a predicted binding energy of −11.26 kcal/mol and a docking-derived Ki estimate of 5.59 nM and was modeled to form hydrogen bonds mainly with Arg44 and Cys41. Sophoricoside also showed a favorable docking score for COX-2, with a predicted binding energy of −10.43 kcal/mol and a docking-derived Ki estimate of 22.47 nM.

In comparison, torachrysone-8-O-β-D-glucopyranoside and triptophenolide showed less favorable docking scores, with predicted binding energies of −8.96 and −8.40 kcal/mol and docking-derived Ki estimates of 271.64 and 691.55 nM, respectively. Honokiol and rhein had less favorable docking-derived Ki estimates in the micromolar range.

Overall, hesperidin and naringin showed comparatively favorable predicted interaction patterns with COX-2 under the applied docking conditions. Together with their protein-associated retention in the COX-2 and CXCL1 ultrafiltration assays, these findings

prioritize the compounds for further investigation. The docking and ultrafiltration results do not establish high-affinity binding, functional target engagement, or a target-specific mechanism of action.

3.4. In Vitro Evaluation of Inflammatory Cytokine Responses

We used LPS-stimulated THP-1-derived macrophages to assess the effects of the selected compounds on inflammatory cytokine levels (Figures 4 and 5). The results showed that following LPS stimulation, the levels of IL-1β, IL-6, and TNF-α were significantly elevated. After treatment with the four compounds (6-methyl-aloe-emodin, rhein, hesperidin, and naringin), the levels of these inflammatory cytokines decreased to varying extents across the tested concentrations. Among them, 6-methyl-aloe-emodin showed the largest reduction in IL-6, rhein showed the largest reduction in IL-1β, and naringin showed the largest reduction in TNF-α. In contrast, hesperidin was associated with reductions in all three measured cytokines. In summary, treatment with the four compounds was associated with reductions in the measured cytokine levels. These findings indicate a preliminary cytokine-modulating effect.

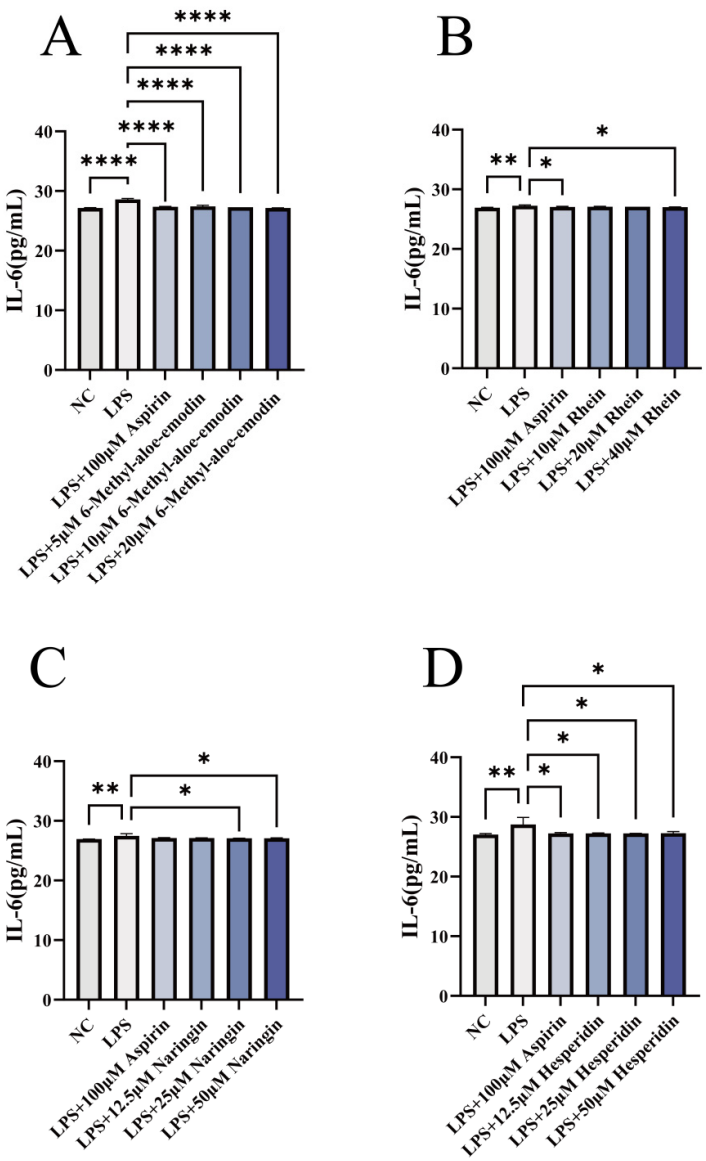


Figure 4. IL-6 levels in LPS-stimulated THP-1-derived macrophages after treatment with the selected compounds. Panels (**A–D**) show IL-6 levels after treatment with 6-methyl-aloe-emodin, rhein,

naringin, and hesperidin, respectively. Statistical significance is indicated as follows: $p < 0.05$ (*), $p < 0.01$ (**), and $p < 0.0001$ (****).

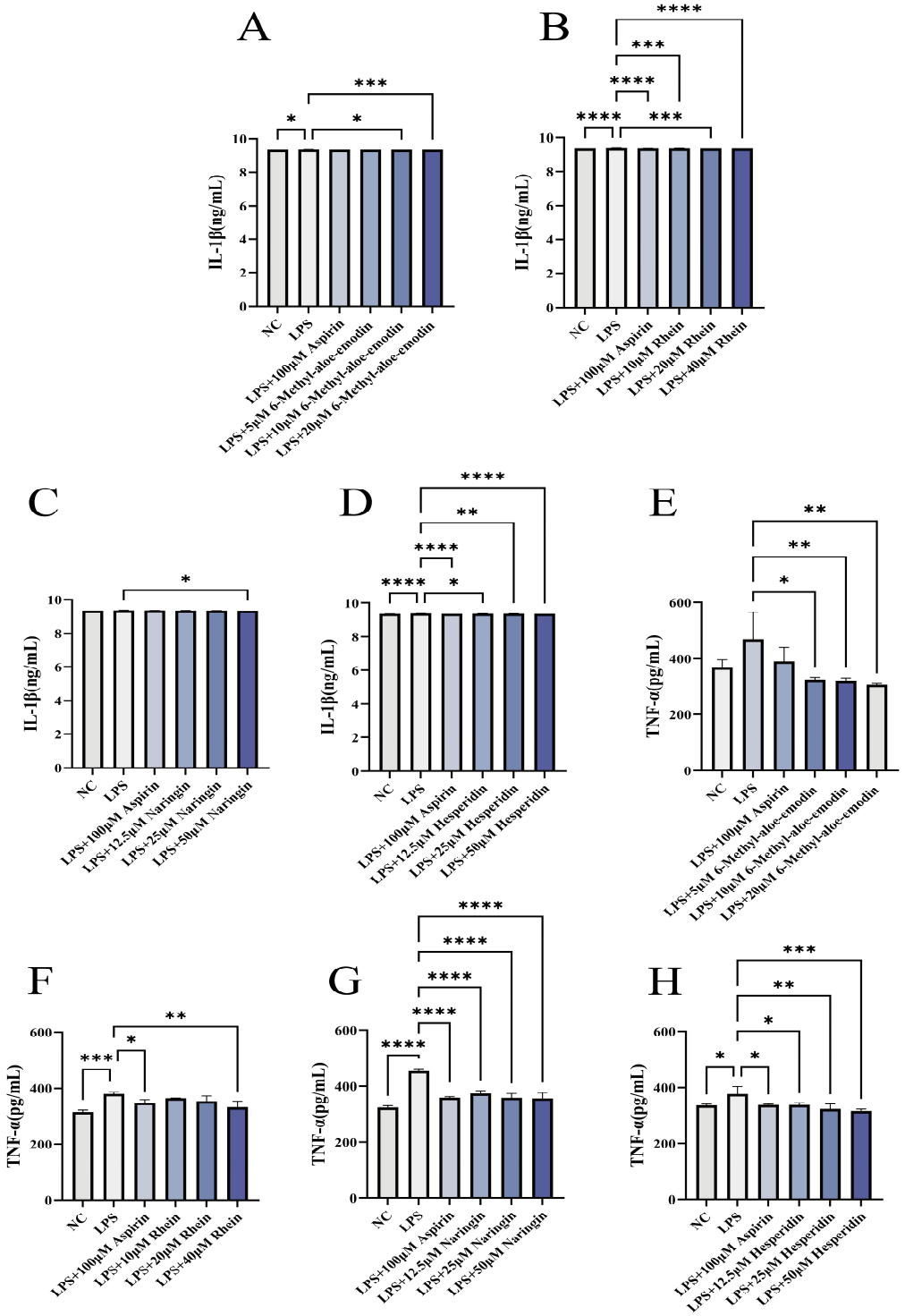


Figure 5. IL-1β and TNF-α levels in LPS-stimulated THP-1-derived macrophages after treatment with the selected compounds. Panels (**A**–**D**) show IL-1β levels after treatment with 6-methyl-aloe-emodin, rhein, naringin, and hesperidin, respectively. Panels (**E**–**H**) show TNF-α levels after treatment with the same compounds, respectively. Statistical significance is indicated as follows: $p < 0.05$ (*), $p < 0.01$ (**), and $p < 0.001$ (***), $p < 0.0001$(****).

4. Discussion

DCQT is a classical Chinese medicine formula used to treat conditions such as excess heat with stagnation, dry stools and constipation, abdominal bloating, pain, and impaired gastrointestinal motility. Modern pharmacological studies have investigated the effects of DCQT on bowel motility, gut function, inflammation, immune responses, oxidative stress, and intestinal tissue repair [30,31]. Previous studies have demonstrated the anti-inflammatory role of DCQT in intestinal obstruction. Proposed mechanisms include modulation of the PI3K/AKT and NF-κB signaling pathways, which may reduce the release of pro-inflammatory mediators such as IL-6, TNF-α, and IL-1β, while also decreasing the infiltration of inflammatory cells [11,32]. Additionally, DCQT modulates the expression of aquaporins (AQP-1 and AQP-5). These changes may affect intestinal barrier function and fluid balance, contributing to the reduction in inflammation and associated tissue damage [33].

This study systematically screened potentially active constituents in DCQT using protein affinity ultrafiltration coupled with LC-MS and molecular docking. The LC-MS analysis yielded 21 putative annotations in negative-ion mode and 18 in positive-ion mode. Figure 6 summarizes the features recovered in the COX-2 and CXCL1 assays. Flavonoid glycosides, including hesperidin and naringin, and anthraquinones, including rhein and 6-methyl-aloe-emodin, were prioritized for further evaluation [34,35]. The screening results are consistent with reports of anti-inflammatory activity for DCQT, although they do not establish a multi-target mechanism. This work extends previous studies of cell-based responses and the overall pharmacological effects of DCQT [11]. UF-LC-MS prioritized DCQT constituents showing protein-associated enrichment for further investigation. However, the use of heat-treated proteins as comparative controls has inherent limitations because heating may alter protein conformation and change nonspecific ligand retention. Although the native-protein and heat-treated-protein preparations were processed under identical conditions and washed repeatedly to reduce background retention, nonspecific adsorption to the protein, ultrafiltration membrane, or device surfaces cannot be completely excluded. Therefore, the BD values were interpreted as relative protein-associated retention signals rather than evidence of specific binding or quantitative binding affinity.

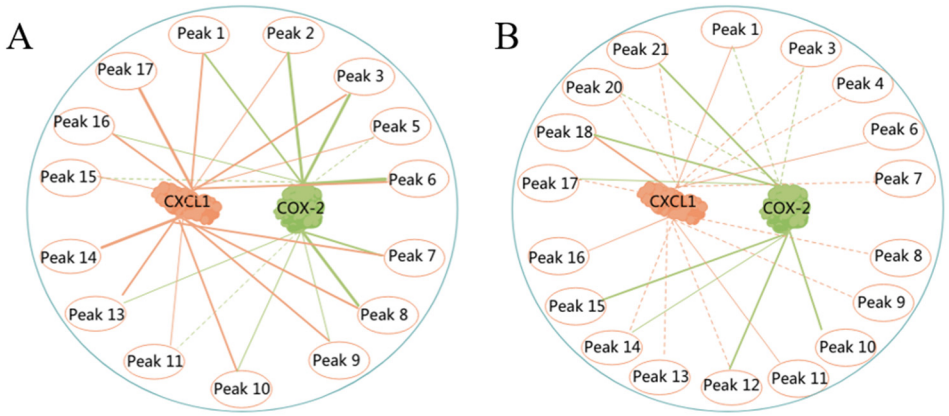


Figure 6. Network of LC–MS features retained in the COX-2 and CXCL1 affinity ultrafiltration assays. (**A**) denotes positive-ion mode, and (**B**) denotes negative-ion mode. Line thickness represents the reported binding degree rather than a measured binding affinity.

The principal analytical contribution of the UF-LC-MS workflow is the introduction of protein-directed separation before chromatographic analysis. Conventional LC-MS profiling describes the chemical composition of an extract but does not indicate which

detected constituents are preferentially retained in the presence of a selected protein. In the present workflow, the DCQT extract was incubated separately with COX-2 or CXCL1, after which ultrafiltration separated protein-associated constituents from unbound small molecules according to molecular size. Following repeated washing, the retained constituents were dissociated, recovered, separated by reversed-phase LC, and detected by Q-TOF-MS/MS [15–18,36]. The workflow therefore provides three successive levels of analytical discrimination: protein-associated enrichment, molecular-size separation, and chromatographic and mass-spectrometric resolution. Its operational selectivity was assessed by comparing the peak areas recovered from native-protein and heat-treated-protein groups. Accordingly, the BD value represents preferential recovery of an LC-MS feature in the native-protein group rather than a direct measurement of target-specific binding affinity [36]. Compared with conventional LC-MS profiling, UF-LC-MS adds protein-directed candidate prioritization to chemical characterization [36]. Compared with bioassay-guided fractionation, it requires less sample, avoids repeated fractionation, and permits the simultaneous evaluation of multiple constituents in a complex extract [36,37]. Compared with immobilized-target ligand-fishing methods, solution-phase incubation avoids chemical immobilization of the protein and reduces immobilization-related steric restrictions [38]. In contrast to molecular docking alone, the ultrafiltration experiment provides evidence of differential protein-associated retention, although it does not establish a binding site or functional effect. The workflow also has important limitations: BD values may be influenced by compound abundance, nonspecific protein association, membrane or device adsorption, washing efficiency, protein conformation, and the selected molecular-weight cutoff. Moreover, heat-inactivated proteins are imperfect controls, and the present workflow does not provide equilibrium binding constants, binding stoichiometry, binding-site information, or evidence of functional inhibition. It should therefore be regarded as a screening and candidate-prioritization method rather than a quantitative binding or target-validation assay. Previous studies have implicated NF-κB and MAPK signaling in the effects of DCQT [9]. Here, hesperidin and naringin showed protein-associated retention in the COX-2 and CXCL1 assays, and the selected compounds reduced inflammatory cytokine levels in a cell model. These findings support further investigation of the prioritized constituents.

Recent studies published in the Journal of Analysis and Testing provide relevant examples of analytical strategies for natural-product research. Bio-affinity ultrafiltration coupled with LC-MS/MS has been used to prioritize protein-associated constituents from medicinal plants [39,40]. A multiple-network analysis integrating metabolomics and pharmacology has also been applied to a traditional Chinese medicine formula for constipation [41]. Recent work on emodin metabolites illustrates how detailed MS/MS analysis can help resolve positional isomers [42], while miniature mass spectrometry has been used to authenticate herbal materials [43]. These reports provide relevant methodological context for the present analytical strategy. They do not, however, validate the identities of the compounds or target interactions reported here; the binding-degree values remain screening signals, and the LC–MS annotations remain putative in the absence of confirmation with authentic standards.

COX-2 plays a well-established role in inflammation by converting arachidonic acid (AA) into prostaglandin E2 (PGE2), which triggers vasodilation, attracts inflammatory cells, and enhances pain sensitivity [4]. Elevated COX-2 levels are observed in postoperative ileus (POI) and inflammatory bowel disease (IBD), contributing to persistent inflammation and intestinal barrier damage [44]. Therefore, targeting COX-2 is a key strategy for alleviating inflammation in POI. Although selective COX-2 inhibitors such as celecoxib are effective, long-term use may pose cardiovascular risks [45]. Whether natural compounds offer a safer alternative requires further evaluation.

Molecular docking predicted favorable interaction patterns between hesperidin or naringin and COX-2. Hesperidin showed a predicted binding energy of −11.76 kcal/mol and formed multiple predicted hydrogen bonds with residues including Tyr130, Gly135, Glu46, Cys47, Cys41, Ser548, Met48, and Asn34. Naringin showed a predicted binding energy of −11.26 kcal/mol and was modeled to interact mainly with Arg44 and Cys41. Their docking-derived Ki estimates were 2.40 and 5.59 nM, respectively. These values are computational estimates intended only for relative comparison under the same docking protocol and should not be interpreted as experimentally measured binding affinities or evidence of direct COX-2 inhibition. Accordingly, hesperidin and naringin were considered candidate compounds for further investigation of their potential interactions with COX-2.

Previous studies have reported anti-inflammatory effects of hesperidin, naringin, rhein, and related anthraquinones in different experimental models. Hesperidin has been shown to reduce oxidative stress, inflammatory-cell recruitment, and the production of selected inflammatory mediators in macrophage and animal models [46–49]. Naringin has been reported to reduce IL-6, IL-1β, and TNF-α levels and to regulate NF-κB-, PPARγ-, and macrophage-polarization-related processes [46,50–53]. Rhein has also been associated with reductions in inflammatory cytokines through mechanisms involving NF-κB, NLRP3, MAPK, Nrf2-related redox regulation, and macrophage activation [36–38,54]. The reductions in IL-6, IL-1β, and TNF-α observed in the present study are broadly consistent with these previously reported anti-inflammatory effects. However, because these studies used different compounds, cell types, stimulation conditions, and experimental endpoints, the present cytokine results do not demonstrate involvement of the same signaling pathways. Moreover, because COX-2 activity, PGE_2 production, CXCL1 secretion, and CXCR2 signaling were not directly measured, the observed cytokine changes cannot be attributed specifically to COX-2 or CXCL1 pathway inhibition. The main contribution of the present study is the application of an integrated workflow to prioritize candidate constituents directly from the chemically complex DCQT extract. In contrast to studies focusing on individual purified compounds or the overall pharmacological effects of the complete formula, protein-affinity ultrafiltration coupled with LC–MS enabled the enrichment and preliminary prioritization of constituents showing protein-associated retention in the presence of COX-2 or CXCL1. Molecular docking provided complementary predictions of possible interaction patterns, and the cell-based assays assessed the effects of selected candidates on inflammatory cytokine levels. This combined strategy efficiently narrows the range of candidate constituents for subsequent investigation; however, it remains a screening and hypothesis-generating approach and does not establish direct target engagement or a target-specific molecular mechanism.

CXCL1 is a pro-inflammatory chemokine that promotes leukocyte recruitment and activation primarily through CXCR2, thereby contributing to inflammatory responses and angiogenesis [54]. Elevated CXCL1 expression has been reported in inflammatory bowel disease, chronic obstructive pulmonary disease, and rheumatoid arthritis [54], making the CXCL1-CXCR2 axis a potential anti-inflammatory target [55]. CXCL1 has also been implicated in ileus-associated inflammation and impaired intestinal contractility [5]; therefore, it was included as an exploratory screening protein in the present study. Hesperidin and naringin showed apparent retention in the CXCL1 UF-LC-MS assay. These findings indicate protein-associated retention under the assay conditions but do not establish specific binding or functional inhibition. Because CXCL1 release and CXCR2 signaling were not measured in the cell assays, the observed cytokine changes cannot be attributed to inhibition of the CXCL1 pathway.

Flavonoid glycosides possess relatively large molecular structures and multiple functional groups that may enable them to form several noncovalent contacts with protein surfaces. In the present study, the affinity ultrafiltration and molecular docking results

suggested possible interactions of hesperidin and naringin with COX-2 and CXCL1. These findings provide hypotheses for further investigation of their potential effects on COX-2-related prostaglandin biosynthesis and CXCL1-CXCR2-related inflammatory signaling. However, the present results do not establish functional dual-target inhibition. Further target-specific and in vivo studies are required to determine the biological relevance of these predicted interactions and whether simultaneous modulation of the two pathways offers any advantage over single-target approaches. Cell viability was not measured at every concentration used in the cytokine assays, so cytotoxicity cannot be fully excluded as a contributor to the observed decreases in cytokine levels.

The UF-LC-MS screening detected multiple features with protein-associated retention, but their chemical identities and pharmacological relevance vary in confidence. Hesperidin, naringin, and hesperetin warrant further investigation because they showed elevated BD values and have reported anti-inflammatory activities. The present data do not establish their target specificity or exclude assay interference. The anthraquinones 6-methyl-aloe-emodin and rhein also reduced measured cytokine levels in the present cell assays. Their assay behavior and target engagement require separate validation. Other provisionally annotated features, including isosinensetin, honokiol, and limonin, showed intermediate BD values but lack independent validation. Low BD values or broad occurrence in natural products are insufficient to establish target specificity or a lack of biological activity for other features. The assignments of N-biotinyl-4-aminobenzoic acid, triptophenolide, forsythoside I, calceolarioside B, certain alkaloids, and atypical acylcarnitines remain uncertain. These low-confidence features should not be treated as confirmed DCQT constituents or used to support target-specific conclusions. Hesperidin, naringin, and hesperetin remain candidates for confirmation with authentic standards and orthogonal biological assays.

This study screened and prioritized candidate anti-inflammatory constituents of DCQT using COX-2 and CXCL1 protein affinity ultrafiltration coupled with LC–MS and molecular docking. Future work should confirm compound identities and target engagement, assess cell viability across the tested concentrations, and evaluate biological relevance in suitable in vivo models [56]. This study provides preliminary analytical evidence for the further investigation of candidate anti-inflammatory constituents in DCQT.

5. Conclusions

This study employed an integrated workflow combining protein-affinity ultrafiltration coupled with LC–MS, molecular docking against COX-2, and cell-based assays to prioritize candidate constituents from Dachengqi Tang (DCQT). Hesperidin and naringin showed protein-associated retention in the COX-2 and CXCL1 ultrafiltration assays and favorable predicted interaction patterns with COX-2 in molecular docking. In LPS-stimulated THP-1-derived macrophages, treatment with 6-methyl-aloe-emodin, rhein, naringin, and hesperidin was associated with reduced levels of IL-6, IL-1β, and TNF-α. These findings provide preliminary evidence of cytokine-modulating effects and warrant further investigation. These cytokine changes do not establish COX-2 or CXCL1 as functional cellular targets, and the proposed target-specific effects require further experimental confirmation. Overall, this study provides preliminary evidence for prioritizing potentially active constituents in DCQT and may serve as a reference for affinity-screening studies of complex natural medicines.

Author Contributions: P.C.: Investigation, Data curation, Formal analysis, Visualization, Writing—original draft, Writing—review & editing. X.H.: Investigation, Data curation, Formal analysis, Writing—review & editing. Z.W. (Zhou Wu): Investigation, Validation, Writing—review & editing. R.F.: Investigation, Methodology, Validation, Writing—review & editing. M.Z.: Investigation, Validation,

Writing—review & editing. J.Z.: Investigation, Resources, Writing—review & editing. Z.W. (Ziqing Wu): Investigation, Data curation, Formal analysis, Writing—review & editing. L.N.: Conceptualization, Methodology, Supervision, Writing—review & editing. X.D.: Conceptualization, Funding acquisition, Project administration, Supervision, Writing—review & editing. M.G.: Conceptualization, Resources, Project administration, Supervision, Writing—review & editing. All authors have read and agreed to the published version of the manuscript.

Funding: This work was partly supported by Medical Scientific Research Foundation of Zhejiang Province, China (2024KY1551, 2025KY1386, 2025KY1503) and the Science and Technology Innovation Yongjiang 2035 Key Research and Development Project of Ningbo (2024Z229). Lutfun Nahar gratefully acknowledges the support from the European Regional Development Fund (Project ENOCH #CZ.02.1.01/0.0/0.0/16_019/0000868), the Czech Science Foundation (Project #23-05474S), and the Chinese Academy of Sciences (PIFI Project #2025PVA0074).

Data Availability Statement: The original contributions presented in this study are included in the article. Further inquiries can be directed to the corresponding authors.

Conflicts of Interest: The authors declare no conflicts of interest.

Abbreviations

The following abbreviations are used in this manuscript:

DCQT	DaChengqi Tang
POI	Postoperative ileus
COX-2	cyclooxygenase-2
UF-LC-MS	ultrafiltration coupled with liquid chromatography–mass spectrometry
PGE_2	prostaglandin E_2
PGG2	prostaglandin G2
PGH2	prostaglandin H2
TCM	traditional Chinese medicine
LPS	lipopolysaccharide
BD	The binding degree
IL-6	Interleukin-6
TNF-α	Tumor Necrosis Factor-α
NF-κB	Nuclear factor kappa-B
IL-1β	Interleukin-1β
AA	arachidonic acid
COPD	chronic obstructive pulmonary disease

References

1. Buscail, E.; Deraison, C. Postoperative ileus: A pharmacological perspective. *Br. J. Pharmacol.* **2022**, *179*, 3283–3305. https://doi.org/10.1111/bph.15800.
2. Lu, W.; Yang, L.; Schulberg, J.D. An unusual cause of small bowel obstruction. *Gastroenterology* **2024**, *166*, 255–258. https://doi.org/10.1053/j.gastro.2023.09.045.
3. Stakenborg, N.; Viola, M.F.; Boeckxstaens, G.E. Intestinal neuro-immune interactions: Focus on macrophages, mast cells and innate lymphoid cells. *Curr. Opin. Neurobiol.* **2020**, *62*, 68–75. https://doi.org/10.1016/j.conb.2019.11.020.
4. Placzek, M.S.; Wilton, D.K.; Weiwer, M.; Manter, M.A.; Reid, S.E.; Meyer, C.J.; Campbell, A.J.; Bajrami, B.; Bigot, A.; Bricault, S.; et al. A fast-binding, functionally reversible, COX-2 radiotracer for CNS PET imaging. *ACS Cent. Sci.* **2024**, *10*, 1105–1114. https://doi.org/10.1021/acscentsci.3c01564.
5. Docsa, T.; Bhattarai, D.; Sipos, A.; Wade, C.E.; Cox, C.S., Jr.; Uray, K. CXCL1 is upregulated during the development of ileus resulting in decreased intestinal contractile activity. *Neurogastroenterol. Motil.* **2020**, *32*, e13757. https://doi.org/10.1111/nmo.13757.
6. Gonfa, Y.H.; Tessema, F.B.; Bachheti, A.; Rai, N.; Tadesse, M.G.; Singab, A.N.; Chaubey, K.K.; Bachheti, R.K. Anti-inflammatory activity of phytochemicals from medicinal plants and their nanoparticles: A review. *Curr. Res. Biotechnol.* **2023**, *6*, 100152. https://doi.org/10.1016/j.crbiot.2023.100152.

7. Arora, C.; Verma, D.K.; Aslam, J.; Mahish, P.K. (Eds.) *Phytochemicals in Medicinal Plants: Biodiversity, Bioactivity and Drug Discovery*; De Gruyter: Berlin, Germany; Boston, MA, USA, 2023. https://doi.org/10.1515/9783110791891.
8. Padalia, R.C.; Verma, D.K.; Arora, C.; Mahish, P.K. (Eds.) *Essential Oils: Sources, Production and Applications*; De Gruyter: Berlin, Germany; Boston, MA, USA, 2023. https://doi.org/10.1515/9783110791600.
9. Zhong, S.; Sun, Y.Q.; Huo, J.X.; Xu, W.Y.; Yang, Y.N.; Yang, J.B.; Wu, W.J.; Liu, Y.X.; Wu, C.M.; Li, Y.G. The gut microbiota-aromatic hydrocarbon receptor (AhR) axis mediates the anticolitic effect of polyphenol-rich extracts from Sanghuangporus. *iMeta* **2024**, *3*, e180. https://doi.org/10.1002/imt2.180.
10. Li, D.; Lv, B.; Wang, D.; Xu, D.; Qin, S.; Zhang, Y.; Chen, J.; Zhang, W.; Zhang, Z.; Xu, F. Network pharmacology and bioactive equivalence assessment integrated strategy driven Q-markers discovery for Da-Cheng-Qi decoction to attenuate intestinal obstruction. *Phytomedicine* **2020**, *72*, 153236. https://doi.org/10.1016/j.phymed.2020.153236.
11. Sun, W.; Chen, Y.; Li, H.; Liu, H.; Li, J.; Chen, J.; Feng, D. Material basis and molecular mechanisms of Dachengqi decoction in the treatment of acute pancreatitis based on network pharmacology. *Biomed. Pharmacother.* **2020**, *121*, 109656. https://doi.org/10.1016/j.biopha.2019.109656.
12. Hu, X.; Liu, S.; Zhu, J.; Ni, H. Dachengqi decoction alleviates acute lung injury and inhibits inflammatory cytokines production through TLR4/NF-κB signaling pathway in vivo and in vitro. *J. Cell. Biochem.* **2019**, *120*, 8956–8964. https://doi.org/10.1002/jcb.27615.
13. Shi, D.; Liu, L.; Li, H.; Pan, D.; Yao, X.; Xiao, W.; Yao, X.; Yu, Y. Identifying the molecular basis of Jinhong tablets against chronic superficial gastritis via chemical profile identification and symptom-guided network pharmacology analysis. *J. Pharm. Anal.* **2022**, *12*, 65–76. https://doi.org/10.1016/j.jpha.2021.01.005.
14. Zhang, Y.; Wang, Y. Recent trends of machine learning applied to multi-source data of medicinal plants. *J. Pharm. Anal.* **2023**, *13*, 1388–1407. https://doi.org/10.1016/j.jpha.2023.07.012.
15. Hua, X.W.; Xu, M.J.; Ming, Y.; Zhang, Y.Y.; Ma, J.; Li, C.; Chu, C.; Wu, Z.; Guo, M.Q. Hypoglycemic and hypolipidemic bioactive compounds from edible traditional Chinese medicines and their action of mechanisms explored by multitarget affinity ultrafiltration with liquid chromatography-mass spectrometry. *Food Front.* **2024**, *6*, 65–85. https://doi.org/10.1002/fft2.488.
16. Feng, H.X.; Chen, G.L.; Guo, M.Q. Exploring multifunctional components from Andrographis paniculata by affinity ultrafiltration with three molecular targets. *Food Chem.* **2023**, *404*, 134515. https://doi.org/10.1016/j.foodchem.2022.134515.
17. Fan, M.X.; Chen, G.L.; Guo, M.Q. Potential antioxidative components in Azadirachta indica revealed by bio-affinity ultrafiltration with SOD and XOD. *Antioxidants* **2022**, *11*, 658. https://doi.org/10.3390/antiox11040658.
18. Xu, Y.J.; Chen, G.L.; Guo, M.Q. Potential anti-aging components from Moringa oleifera leaves explored by affinity ultrafiltration with multiple drug targets. *Front. Nutr.* **2022**, *9*, 854882. https://doi.org/10.3389/fnut.2022.854882.
19. Hemavathi, K.N.; Skariyachan, S.; Raju, R.; Keshava Prasad, T.S.; Abhinand, C.S. Computational screening of potential anti-inflammatory leads from Jeevaneeya Rasayana plants targeting COX-2 and 5-LOX by molecular docking and dynamic simulation approaches. *Comput. Biol. Med.* **2024**, *171*, 108164. https://doi.org/10.1016/j.compbiomed.2024.108164.
20. Praveen Kumar, K.; Piramanayagam, S. Molecular docking analysis of antimicrobial peptides with the CXCL1 protein target for colorectal cancer. *Bioinformation* **2021**, *17*, 679–687. https://doi.org/10.6026//97320630017369.
21. Liang, Z.; Sham, T.; Yang, G.; Yi, L.; Chen, H.; Zhao, Z. Profiling of secondary metabolites in tissues from Rheum palmatum L. using laser microdissection and liquid chromatography mass spectrometry. *Anal. Bioanal. Chem.* **2013**, *405*, 4199–4212. https://doi.org/10.1007/s00216-013-6819-z.
22. Feng, J.; Ren, H.; Gou, Q.; Zhu, L.; Ji, H.; Yi, T. Comparative analysis of the major constituents in three related polygonaceous medicinal plants using pressurized liquid extraction and HPLC-ESI/MS. *Anal. Methods* **2016**, *8*, 1557–1564. https://doi.org/10.1039/C5AY02941D.
23. Testai, L.; De Leo, M.; Flori, L.; Polini, B.; Braca, A.; Nieri, P.; Pistelli, L.; Calderone, V. Contribution of irisin pathway in protective effects of mandarin juice (Citrus reticulata Blanco) on metabolic syndrome in rats fed with high fat diet. *Phytother. Res.* **2021**, *35*, 4324–4333. https://doi.org/10.1002/ptr.7128.
24. Sun, Y.; Hou, Z.; Liu, Z.; Wang, J. Ionic liquid-based ultrasonic-assisted extraction of forsythosides from the leaf of Forsythia suspensa (Thunb.) Vahl and subsequent separation and purification by high-speed counter-current chromatography. *J. Chromatogr. Sci.* **2016**, *54*, 1445–1452. https://doi.org/10.1093/chromsci/bmw069.
25. He, X.G.; Lian, L.Z.; Lin, L.Z.; Bernart, M.W. High-performance liquid chromatography–electrospray mass spectrometry in phytochemical analysis of sour orange (*Citrus aurantium* L.). *J. Chromatogr. A* **1997**, *791*, 127–134. https://doi.org/10.1016/S0021-9673(97)00779-6.

26. Abdallah, H.M.; Al-Abd, A.M.; Asaad, G.F.; Abdel-Naim, A.B.; El-halawany, A.M. Isolation of antiosteoporotic compounds from seeds of Sophora japonica. *PLoS ONE* **2014**, *9*, e98559. https://doi.org/10.1371/journal.pone.0098559.
27. Tang, W.; Wan, M.; Zhu, Z.; Chen, G.; Huang, X. Simultaneous determination of eight major bioactive compounds in Dachengqi Tang (DT) by high-performance liquid chromatography. *Chin. Med.* **2008**, *3*, 5. https://doi.org/10.1186/1749-8546-3-5.
28. Xu, F.; Liu, Y.; Song, R.; Dong, H.; Zhang, Z. Constituents of Da-Cheng-Qi decoction and its parent herbal medicines determined by LC-MS/MS. *Nat. Prod. Commun.* **2010**, *5*, 789–794. https://doi.org/10.1177/1934578X1000500522.
29. He, Y.; Li, Z.; Wang, W.; Sooranna, S.R.; Shi, Y.; Chen, Y.; Wu, C.; Zeng, J.; Tang, Q.; Xie, H. Chemical profiles and simultaneous quantification of Aurantii fructus by use of HPLC-Q-TOF-MS combined with GC-MS and HPLC methods. *Molecules* **2018**, *23*, 2189. https://doi.org/10.3390/molecules23092189.
30. Bouyahya, A.; Guaouguaou, F.E.; El Omari, N.; El Menyiy, N.; Balahbib, A.; El-Shazly, M.; Bakri, Y. Anti-inflammatory and analgesic properties of Moroccan medicinal plants: Phytochemistry, in vitro and in vivo investigations, mechanism insights, clinical evidences and perspectives. *J. Pharm. Anal.* **2022**, *12*, 35–57. https://doi.org/10.1016/j.jpha.2021.07.004.
31. Li, J.; Dai, Y.; Cao, H.; Xiao, T.; Ge, B.; Xing, L.; Yu, X.; Fu, Z. Dachengqi decoction reduces inflammatory response and promotes recovery of gastrointestinal function in patients with mild acute pancreatitis by regulating the intestinal microbiota. *Zhonghua Wei Zhong Bing. Ji Jiu Yi Xue* **2023**, *35*, 170–176. https://doi.org/10.3760/cma.j.cn121430-20220921-00852.
32. Gandhi, G.R.; Mohana, T.; Athesh, K.; Hillary, V.E.; Vasconcelos, A.B.S.; Farias de Franca, M.N.; Montalvao, M.M.; Ceasar, S.A.; Jothi, G.; Sridharan, G.; et al. Anti-inflammatory natural products modulate interleukins and their related signaling markers in inflammatory bowel disease: A systematic review. *J. Pharm. Anal.* **2023**, *13*, 1408–1428. https://doi.org/10.1016/j.jpha.2023.09.012.
33. Pan, L.Y.; Chen, Y.F.; Li, H.C.; Bi, L.M.; Sun, W.J.; Sun, G.F.; Zhang, X.F.; Xu, K.; Feng, D.X. Dachengqi decoction attenuates intestinal vascular endothelial injury in severe acute pancreatitis in vitro and in vivo. *Cell. Physiol. Biochem.* **2017**, *44*, 2395–2406. https://doi.org/10.1159/000486155.
34. Li, H.; Wang, Y.; Shao, S.; Yu, H.; Wang, D.; Li, C.; Yuan, Q.; Liu, W.; Cao, J.; Wang, X.; et al. Rabdosia serra alleviates dextran sulfate sodium salt-induced colitis in mice through anti-inflammation, regulating Th17/Treg balance, maintaining intestinal barrier integrity, and modulating gut microbiota. *J. Pharm. Anal.* **2022**, *12*, 824–838. https://doi.org/10.1016/j.jpha.2022.08.001.
35. Wongso, H. Natural product-based radiopharmaceuticals: Focus on curcumin and its analogs, flavonoids, and marine peptides. *J. Pharm. Anal.* **2022**, *12*, 380–393. https://doi.org/10.1016/j.jpha.2021.07.006.
36. Chen, G.; Huang, B.X.; Guo, M. Current advances in screening for bioactive components from medicinal plants by affinity ultrafiltration mass spectrometry. *Phytochem. Anal.* **2018**, *29*, 375–386. https://doi.org/10.1002/pca.2769.
37. Kellogg, J.J.; Paine, M.F.; McCune, J.S.; Oberlies, N.H.; Cech, N.B. Selection and characterization of botanical natural products for research studies: A NaPDI Center recommended approach. *Nat. Prod. Rep.* **2019**, *36*, 1196–1221. https://doi.org/10.1039/C8NP00065D.
38. Zhuo, R.; Liu, H.; Liu, N.; Wang, Y. Ligand fishing: A remarkable strategy for discovering bioactive compounds from complex mixtures of natural products. *Molecules* **2016**, *21*, 1516. https://doi.org/10.3390/molecules21111516.
39. Zhang, H.; Chen, G.; Zhang, Y.; Muema, F.W.; Ding, J.; Guo, M. Screening for bioactive compounds from mulberry leaves combining bio-affinity ultrafiltration with α-glucosidase and pancreatic lipase. *J. Anal. Test.* **2024**, *8*, 315–326. https://doi.org/10.1007/s41664-024-00305-2.
40. Fan, M.; Rakotondrabe, T.F.; Chen, G.; Guo, M. Antiparasitic activity and potential active compounds from Azadirachta indica revealed by affinity ultrafiltration chromatography–mass spectrometry with acetylcholinesterase and lactate dehydrogenases. *J. Anal. Test.* **2024**, *8*, 403–414. https://doi.org/10.1007/s41664-024-00315-0.
41. Shi, J.; Xiang, L.; Lam, Y.Y.; Ning, Z.; Liu, J.; Zhou, Y.; Zhai, L.; Lin, C.; Lin, Z. A novel multiple-network analysis integrating metabolomics and pharmacology for mechanism study of medicine: A case study of CDD-2101 against constipation. *J. Anal. Test.* **2024**, *8*, 415–430. https://doi.org/10.1007/s41664-024-00324-z.
42. Li, W.; Li, X.; Wen, J.; Zhu, Z.; Jin, H.; Jia, J.; Wang, Q.; Song, Y. Structural identification of emodin metabolites in rats after oral administration through deciphering positional isomers. *J. Anal. Test.* **2026**, *10*, 1106–1112. https://doi.org/10.1007/s41664-026-00445-7.
43. Xie, Y.; Huang, S.; Zhang, Q.; Zhang, S.; Han, Z.; Yu, J.; Wang, X.; Chen, K.; Wang, Z.; Li, L.; et al. On-site analysis and rapid authentication of valuable agarwood samples by paper capillary spray miniature mass spectrometry. *J. Anal. Test.* **2025**, *9*, 61–70. https://doi.org/10.1007/s41664-024-00331-0.
44. Huang, C.; Xiong, X.; Zhang, D.; Ruan, Q.; Jiang, J.; Wang, F.; Chen, G.; Cheng, L. Targeted screening of multiple anti-inflammatory components from Chrysanthemi indici Flos by ligand fishing with affinity UF-LC/MS. *Front. Pharmacol.* **2024**, *15*, 1272087. https://doi.org/10.3389/fphar.2024.1272087.

45. Choi, J.S.; Ahn, J.B.; Park, J.S. Amorphous multi-system of celecoxib improves its anti-inflammatory activity in vitro and oral absorption in rats. *Int. J. Pharm.* **2019**, *555*, 135–145. https://doi.org/10.1016/j.ijpharm.2018.11.050.
46. De Souza, A.B.F.; de Matos, N.A.; Castro, T.F.; Costa, G.P.; Oliveira, L.A.M.; Nogueira, K.O.P.C.; Ribeiro, I.M.L.; Talvani, A.; Cangussu, S.D.; de Menezes, R.C.A.; et al. Effects in vitro and in vivo of hesperidin administration in an experimental model of acute lung inflammation. *Free Radic. Biol. Med.* **2022**, *180*, 253–262. https://doi.org/10.1016/j.freeradbiomed.2022.01.027.
47. Adefegha, S.A.; Bottari, N.B.; Leal, D.B.; Andrade, C.M.d.; Schetinger, M.R. Interferon gamma/interleukin-4 modulation, anti-inflammatory and antioxidant effects of hesperidin in complete Freund's adjuvant (CFA)-induced arthritis model of rats. *Immunopharmacol. Immunotoxicol.* **2020**, *42*, 509–520. https://doi.org/10.1080/08923973.2020.1814806.
48. Miles, E.A.; Calder, P.C. Effects of citrus fruit juices and their bioactive components on inflammation and immunity: A narrative review. *Front. Immunol.* **2021**, *12*, 712608. https://doi.org/10.3389/fimmu.2021.712608.
49. Heo, S.-D.; Kim, J.; Choi, Y.; Ekanayake, P.; Ahn, M.; Shin, T. Hesperidin improves motor disability in rat spinal cord injury through anti-inflammatory and antioxidant mechanism via Nrf-2/HO-1 pathway. *Neurosci. Lett.* **2020**, *715*, 134619. https://doi.org/10.1016/j.neulet.2019.134619.
50. Ansari, B.; Aschner, M.; Hussain, Y.; Efferth, T.; Khan, H. Suppression of colorectal carcinogenesis by naringin. *Phytomedicine* **2022**, *96*, 153897. https://doi.org/10.1016/j.phymed.2021.153897.
51. Liang, H.; Yang, Q.; Zhong, B.; Li, D.; Wu, F.; Zhang, J.; Guo, C.; Zhu, Z.; Feng, M.; Zhang, Y.; et al. IL-1β+ tumor-associated macrophages accelerate glioblastoma progression by amplifying the PGE2-EP4 signaling. *J. Neuroinflamm.* **2025**, *22*, 233. https://doi.org/10.1186/s12974-025-03551-y.
52. Zhou, Y.; Gao, C.; Vong, C.T.; Tao, H.; Li, H.; Wang, S.; Wang, Y. Rhein regulates redox-mediated activation of NLRP3 inflammasomes in intestinal inflammation through macrophage-activated crosstalk. *Br. J. Pharmacol.* **2022**, *179*, 1978–1997. https://doi.org/10.1111/bph.15773.
53. Liu, Y.; Tang, X.; Yuan, H.; Gao, R. Naringin inhibits macrophage foam cell formation by regulating lipid homeostasis and metabolic phenotype. *Nutrients* **2024**, *16*, 1321. https://doi.org/10.3390/nu16091321.
54. Wang, H.; Yang, D.; Li, L.; Yang, S.; Du, G.; Lu, Y. Anti-inflammatory effects and mechanisms of Rhein, an anthraquinone compound, and its applications in treating arthritis: A review. *Nat. Prod. Bioprospect.* **2020**, *10*, 445–452. https://doi.org/10.1007/S13659-020-00272-Y.
55. Cao, D.L.; Zhang, Z.J.; Xie, R.G.; Jiang, B.C.; Ji, R.R.; Gao, Y.J. Chemokine CXCL1 enhances inflammatory pain and increases NMDA receptor activity and COX-2 expression in spinal cord neurons via activation of CXCR2. *Exp. Neurol.* **2014**, *261*, 328–336. https://doi.org/10.1016/j.expneurol.2014.05.014.
56. Fadaka, A.O.; Akinsoji, T.; Klein, A.; Madiehe, A.M.; Meyer, M.; Keyster, M.; Sikhwivhilu, L.M.; Sibuyi, N.R.S. Stage-specific treatment of colorectal cancer: A microRNA-nanocomposite approach. *J. Pharm. Anal.* **2023**, *13*, 1235–1251. https://doi.org/10.1016/j.jpha.2023.07.008.

Disclaimer/Publisher's Note: The statements, opinions and data contained in all publications are solely those of the individual author(s) and contributor(s) and not of MDPI and/or the editor(s). MDPI and/or the editor(s) disclaim responsibility for any injury to people or property resulting from any ideas, methods, instructions or products referred to in the content.